

See discussions, stats, and author profiles for this publication at: <https://www.researchgate.net/publication/272167663>

# Crystalline ZnO/Amorphous ZnO Core/Shell Nanorods: Self-Organized Growth, Structure and Novel Luminescence

ARTICLE in THE JOURNAL OF PHYSICAL CHEMISTRY C · FEBRUARY 2015

Impact Factor: 4.77 · DOI: 10.1021/jp511783c

CITATIONS

2

READS

157

6 AUTHORS, INCLUDING:



Saikumar Inguva

Dublin City University

4 PUBLICATIONS 13 CITATIONS

SEE PROFILE



Sandeep Kumar Marka

University of Hyderabad

11 PUBLICATIONS 16 CITATIONS

SEE PROFILE



Vadali V S S Srikanth

University of Hyderabad

60 PUBLICATIONS 234 CITATIONS

SEE PROFILE

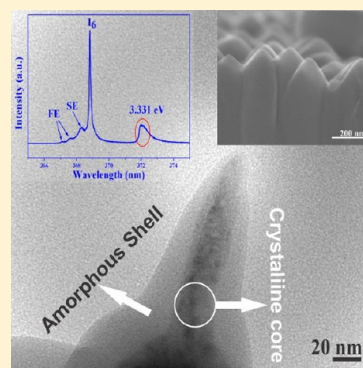
# Crystalline ZnO/Amorphous ZnO Core/Shell Nanorods: Self-Organized Growth, Structure, and Novel Luminescence

Saikumar Inguva,<sup>†,||</sup> Sandeep Kumar Marka,<sup>‡</sup> Rajani K. Vijayaraghavan,<sup>§,||</sup> Enda McGlynn,<sup>†,||</sup> Vadali V. S. S. Srikanth,<sup>‡</sup> and J.-P. Mosnier<sup>\*,†,||</sup>

<sup>†</sup>School of Physical Sciences, <sup>§</sup>School of Electronic Engineering, and <sup>||</sup>National Centre for Plasma Science and Technology, Dublin City University, Glasnevin, Dublin 9, Ireland

<sup>‡</sup>School of Engineering Sciences and Technology, University of Hyderabad, Hyderabad 500046, India

**ABSTRACT:** We have used pulsed-laser deposition, following a specific sequence of heating and cooling phases, to grow ZnO nanorods on ZnO buffer/Si(100) substrates, in a 600 mT oxygen ambient, without catalyst. In these conditions, the nanorods preferentially self-organize in the form of vertically aligned, core/shell structures. X-ray diffraction analyses, obtained from  $2\theta$ - $\omega$  and pole figure scans, shows a crystalline (wurtzite) ZnO deposit with uniform  $c$ -axis orientation normal to the substrate. Field emission scanning electron microscopy, transmission electron microscopy (TEM), high resolution TEM, and selected area electron diffraction studies revealed that the nanorods have a crystalline core and an amorphous shell. The low-temperature (13 K) photoluminescence featured a strong  $I_6$  (3.36 eV) line emission, structured green band emission, and a hitherto unreported broad emission at 3.331 eV. Further studies on the 3.331 eV band showed the involvement of deeply bound excitonic constituents in a single electron-hole recombination. The body of structural data suggests that the 3.331 eV emission can be linked to the range of defects associated with the unique crystalline ZnO/amorphous ZnO core/shell structure of the nanorods. The relevance of the work is discussed in the context of the current production methods of core/shell nanorods and their domains of application.



## 1. INTRODUCTION

Core/shell nanostructures constituted by a variety of materials including metals,<sup>1</sup> semiconductors,<sup>2–4</sup> hydroxides,<sup>5</sup> and organic materials<sup>6</sup> have been attracting significant attention for applications in several interdisciplinary fields such as sensing, multienzyme biocatalysis, drug delivery, and photonics.<sup>7</sup> This is because the core/shell architecture enables the tailoring of novel properties via modification of the functionality, charge or reactivity of the nanostructures surface.<sup>2–4,8</sup> In particular, the enhancement of the luminescent properties of one-dimensional nanostructures can be achieved following this method.<sup>8</sup>

ZnO, a wide direct band gap (3.37 eV) semiconductor, has been used successfully in core/shell architectures due to its excellent material properties<sup>9–11</sup> that include relatively facile nanostructure fabrication. ZnO based core/shell nanostructures including ZnO/Fe<sub>2</sub>O<sub>3</sub>, ZnO/In<sub>2</sub>O<sub>3</sub>,<sup>12,13</sup> ZnO/ZnS, ZnO/ZnTe, ZnO/TiO<sub>2</sub>,<sup>14–17</sup> ZnO/MoO<sub>3</sub>, hydrogenated ZnO,<sup>18,19</sup> and ZnO/NiO<sup>20</sup> have been produced for applications in gas sensors, photovoltaics, supercapacitors, and energy storage, respectively. In this context, ZnO/Bi<sub>2</sub>O<sub>3</sub>,<sup>21</sup> Zn/ZnO,<sup>22,23</sup> and ZnO/Zn(OH)<sub>2</sub><sup>24</sup> core/shell architectures have also been reported.

Core/shell nanostructures are typically fabricated as part of complex multistep processes. In the first step, the nanostructure core is fabricated, followed by the growth of the shell region in a second step, with several intermediate operations and possibly a change of growth method being implemented between these two steps. For example, Greene et al. have fabricated a ZnO nanorod

core in a two-step aqueous process and subsequently prepared a TiO<sub>2</sub> shell by atomic layer deposition.<sup>15</sup> Huang et al. have fabricated a ZnO core and In<sub>2</sub>O<sub>3</sub> shell by an aqueous chemical process and a combination of sputtering and thermal oxidation methods, respectively.<sup>13</sup> Additionally, other growth methods such as hydrolysis,<sup>12,16</sup> electrochemical synthesis,<sup>18</sup> and pulsed laser deposition (PLD)<sup>8,25</sup> have been used by other workers. Of particular interest for the present work, we note the PLD works of Kaydashev et al.<sup>25</sup> and Li et al.,<sup>8</sup> who prepared ZnO/Zn<sub>0.9</sub>Mn<sub>0.1</sub>O and ZnO/Er<sub>2</sub>O<sub>3</sub> core/shell nanorods using multistep growth processes in Ar and/or O<sub>2</sub> ambient pressures with the aid of Au catalyst, respectively.

In this work, we develop a specific catalyst free PLD growth sequence to obtain self-organized ZnO/ZnO core/shell nanorods without the need for a separate growth step for the shell, using as the substrate a Si(100) wafer coated by a thin ZnO buffer layer. We also investigate the structural, morphological, and optical properties of the as-grown ZnO/ZnO core/shell nanorod deposit and the relationship of the latter to the unique defect structure associated with the core/shell architecture.

## 2. EXPERIMENTAL DETAILS

ZnO/ZnO core/shell nanorods were grown using a standard PLD apparatus equipped with a high-power, Q-switched,

Received: November 25, 2014

Revised: February 10, 2015

Published: February 12, 2015

frequency-quadrupled, Nd:YAG laser.<sup>26</sup> The output laser wavelength, repetition rate, pulse width, and energy were 266 nm, 10 Hz, 6 ns, and 150 mJ, respectively. The average fluence delivered at the laser spot was  $\sim 2.0 \text{ J/cm}^2$ . A ZnO (99.999% pure, PI-KEM) sintered ceramic disk of diameter 2.54 cm was used as the target. The target–substrate distance was kept constant at 5 cm. Cleaved  $1 \text{ cm} \times 2 \text{ cm}$  pieces of Si(100) wafers were used as substrates. Prior to deposition, the substrates were degreased/cleaned for 15 min in an ultrasonic bath filled with acetone/isopropyl alcohol. Silver paste was used to mount substrates on the substrate holder in the deposition chamber. Before deposition, the substrates were heated to  $900^\circ\text{C}$  for 30 min for the purpose of surface cleaning using a heater coil and then cooled to  $450^\circ\text{C}$ .

The fabrication of ZnO/ZnO core/shell nanorods on Si(100) wafer substrates involved two stages. The first stage was to prepare a thin ZnO buffer layer. The buffer layer of thickness around 120 nm (5000 laser shots) was deposited at a substrate temperature of  $450^\circ\text{C}$  in an ambient  $\text{O}_2$  pressure of 100 mT. Following deposition of the buffer layer, the substrate temperature was increased to  $700^\circ\text{C}$  at a rate of  $12.5^\circ\text{C/min}$ , then left at this temperature for 5 min, and finally cooled to  $150^\circ\text{C}$  at a rate of  $9.16^\circ\text{C/min}$ . The second stage involved the preparation of the core/shell nanorods. The ZnO buffer/substrate temperature was initially raised to  $800^\circ\text{C}$  at a rate of  $7.22^\circ\text{C/min}$ . The ZnO/ZnO core/shell nanorods were then grown at this temperature in a 600 mT  $\text{O}_2$  pressure and left in these conditions for 5 min. After this period, the substrate temperature was cooled to  $150^\circ\text{C}$  at a rate of  $8.66^\circ\text{C/min}$ . The actual deposition time of the core/shell nanorods was about 2 h (40 000 laser shots), excluding the sequence of heating and cooling phases to pre- and postgrowth. The full length of the core/shell nanorod obtained in these conditions was around  $1 \mu\text{m}$ . Five growths using the same conditions and sequences were performed. The same nanorod architecture was obtained in each case and is thus fully reproducible. From the viewpoint of the growths, we conclude that the overall sequence of specific heating and cooling phases used in this work has allowed us to achieve self-organized core/shell architecture, without the need for a separate growth step for the shell region. The self-organization of ZnO nanostructures is a known feature of this material.<sup>27</sup> Also, to the best of our knowledge, similar growths of ZnO nanorods<sup>28,29</sup> carried out in similar pressure conditions all lead to a simple nanorod structure, i.e., without a shell. Thus, we can conclude that the series of substrate temperatures for the given deposition rate used in this PLD work should be the important parameter influencing the growth mode and kinetics<sup>30</sup> that lead to the formation of the core/shell architecture.

The structural characteristics were investigated by  $2\theta$ – $\omega$  and pole figure X-ray diffraction scans (XRD; Bruker AXS D8 Advance and Jordan Valley BEDE-D1 diffractometers), respectively. The surface morphologies and nanostructures were studied by scanning electron microscopy (SEM; Carl-Zeiss EVO series), field emission SEM (FE-SEM; Hitachi S5500), and transmission electron microscopy (TEM; FEI Technai G<sup>2</sup> S-Twin, operating voltage of 200 kV). High resolution TEM (HR-TEM) and selected area electron diffraction (SAED) were studied using the same TEM apparatus. Low-temperature photoluminescence (PL) spectra were recorded (with 1 m Model SPEX 1701 monochromator) using 332 nm He–Cd laser excitation.

### 3. RESULTS AND DISCUSSION

**3.1. Structural Properties.** Figure 1 shows the  $2\theta$ – $\omega$  XRD scan, on a log scale, for ZnO/ZnO core/shell nanorods (black

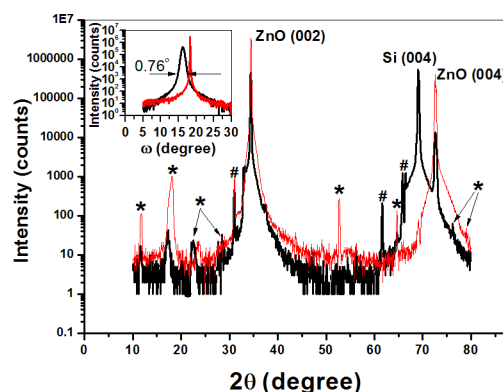


**Figure 1.**  $2\theta$ – $\omega$  XRD scans for ZnO/ZnO core/shell nanorods (black line) and a ZnO single crystal wafer (red line) (The features marked with \* are due to the adhesive mounting tape used. The features marked with # are due to Cu  $K\beta$  and tungsten  $L\alpha$  radiations from the X-ray tube, with the latter due to contamination.) The inset shows the rocking curve scans from the two samples around the ZnO(002) peak position.

line) grown by PLD and similar data from a ZnO single crystal wafer (red line). The ZnO/ZnO core/shell nanorods show a dominant (002) reflection at  $2\theta \approx 34.40^\circ$  and a weaker (004) reflection at  $2\theta \approx 72.62^\circ$ . The origin of the weaker or impurity features is also mentioned in the Figure 1 caption. No other ZnO-related peaks are observable. The intensity of the PLD-deposited ZnO(002) reflection is around 1 million counts. The ZnO/ZnO core/shell nanorods grown by PLD on Si(100) substrates are clearly highly textured and oriented with their  $c$ -axes normal to the substrate surface. These data are similar to observations (including the identification of the weaker/impurity peaks) made previously by us and also by others.<sup>31–33</sup> For comparison, we have measured a  $2\theta$ – $\omega$  XRD scan using a  $c$ -plane terminated ZnO single crystal wafer of thickness 0.5 mm (Tokyo Denpa) using the same conditions (red line in Figure 1). The measured  $2\theta$  value for the ZnO single crystal (002) reflection is  $\approx 34.45^\circ$ , identical to the value for our nanorods ( $\approx 34.40^\circ$ ). We have also measured the fwhm of the ZnO(002) reflection for the PLD-deposited ZnO, and we used these  $2\theta$  and fwhm values to calculate the  $c$ -axis lattice spacing and crystallite size (more accurately, the out-of-plane coherence length), using Bragg's law and the Scherrer equation corrected for instrumental broadening, respectively (we use the weighted average value of the wavelengths of Cu  $K\alpha_1$  and Cu  $K\alpha_2$  radiation lines for the X-ray wavelength in all calculations, i.e.,  $\lambda = 1.5425 \text{ \AA}$ ). The details of the calculation are discussed in a previous article, including the correction for the instrumental response when using the Scherrer equation.<sup>34</sup> The PLD-deposited ZnO(002) reflection fwhm,  $c$ -axis lattice spacing, and crystallite size values are  $0.198^\circ$ ,  $5.216 \text{ \AA}$ , and  $75.31 \text{ nm}$ , respectively. The  $c$ -axis lattice spacing value is comparable with the value calculated for the ZnO single crystal wafer ( $5.207 \text{ \AA}$ ). We note that the value of the lattice spacing ( $c$ ) obtained from the aforementioned single crystal value of  $2\theta = 34.45^\circ$  matches precisely the published ZnO  $c$ -axis lattice spacing of  $5.20690 \text{ \AA}$  (JCPDS Card No. 36-1451) when rounded off to the third decimal place.

The inset of Figure 1 shows the rocking curve for the (002) reflection from the ZnO/ZnO core/shell nanorod sample (black



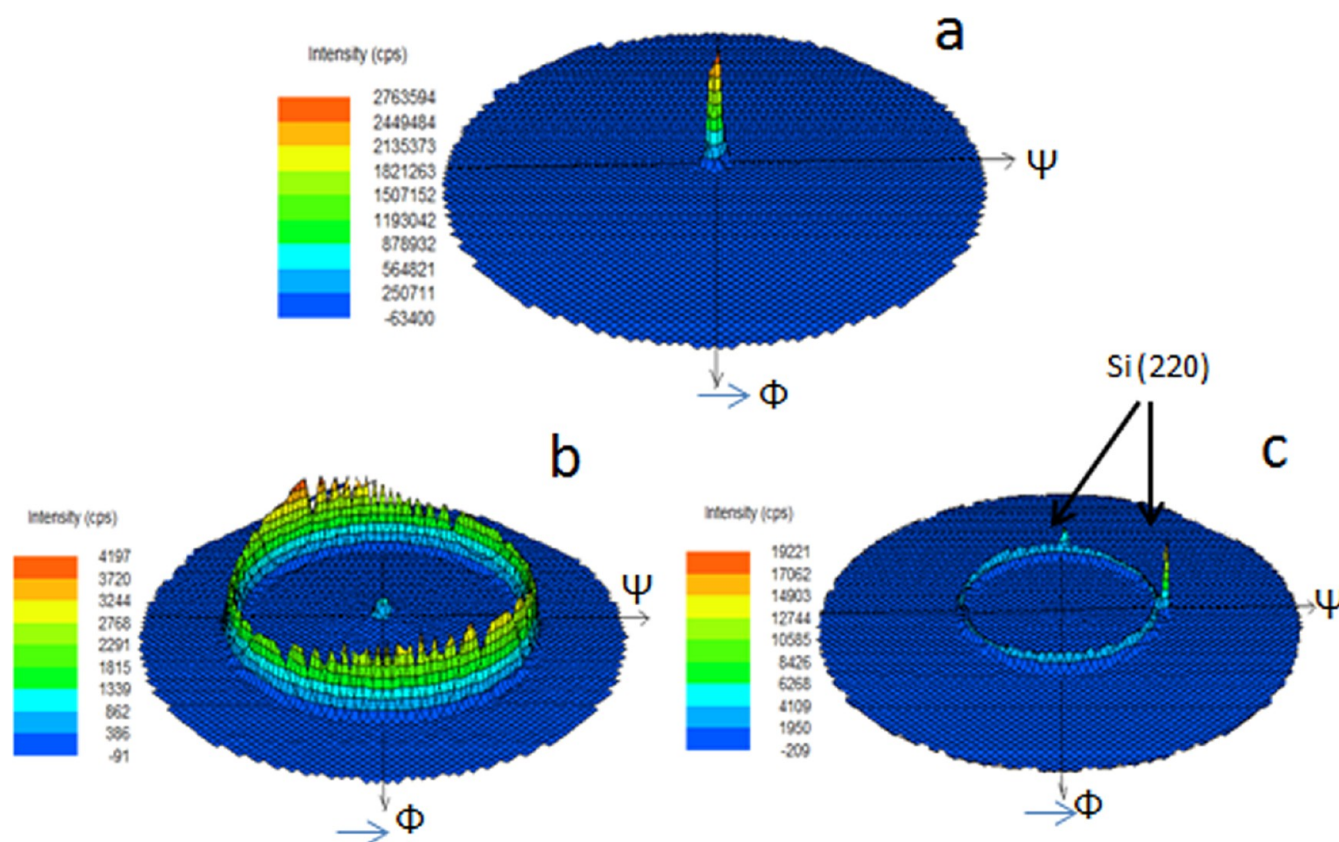


**Figure 2.** XRD pole figures for the (a) (002), (b) (101), and (c) (102) ZnO planes, respectively, in ZnO/ZnO core/shell nanorods grown by PLD.

line) and for the (002) reflection from the ZnO single crystal wafer (red line). The rocking curve of the ZnO/ZnO core/shell nanorods sample has a fwhm of  $0.76^\circ$ , which is notably smaller than the data on samples of a similar type reported previously for ZnO nanorods.<sup>31,32,35</sup> This, together with the  $2\theta$ - $\omega$  data, indicates excellent crystallite alignment and texture. We note that, as expected, the fwhm of the rocking curve for the ZnO single crystal wafer is much narrower, essentially limited by the instrument broadening ( $<0.1^\circ$ ). Since no catalyst or crystalline phases are identified in the XRD data. In conclusion, the XRD analyses confirm that the ZnO/ZnO core/shell nanorod deposit grown by PLD on Si(100) substrates is well-aligned with excellent  $c$ -axis orientation normal to the substrate surface.

XRD pole figure analyses were also used to undertake a more detailed investigation of the texture and in-plane orientation of the ZnO/ZnO core/shell nanorods. Pole figures of the (002), (101), and (102) planes were measured at  $2\theta$  values of  $34.5^\circ$ ,  $36.5^\circ$ , and  $47.5^\circ$ , respectively (Figure 2). Figure 2a shows a narrow and intense (002) pole figure centered at  $\Psi = 0$  indicating the growth of the core/shell nanorods with their vertical axes along the substrate normal. Figures 2b,c shows rotationally (circularly) symmetric (101) and (102) pole figures at  $\Psi$  angle values of  $\sim 62.7^\circ$  and  $\sim 42.9^\circ$ , respectively. The latter are very close to the values of the angles between the ZnO(101)/(002) and ZnO(102)/(002) planes, as expected from the known crystallographic structure of ZnO.<sup>36,37</sup> The intense spots at  $\Psi = 45^\circ$  on the (102) pole figure, indicated in Figure 2c, are due to the (220) planes of the Si substrate, and were seen previously.<sup>36</sup> The pole figure data confirm that the PLD-grown ZnO/ZnO core/shell nanorods are well textured with excellent vertical orientation along the  $c$ -axis and also show the complete

absence of any in-plane orientation, i.e., the absence of epitaxy, on the substrate.

**3.2. Surface Morphology and Nanostructuring.** The surface morphologies of the core/shell nanorod deposits were studied using SEM, FE-SEM, and TEM. Figure 3a,b,d shows FE-SEM images, and Figure 3c shows an SEM image, taken at various tilt angles. These images show that the core/shell nanorods have almost conical terminations with rounded or blunt tips. Figure 3 also strongly supports the conclusions from XRD ( $2\theta$ - $\omega$  and X-ray pole figures) analysis concerning the preferred  $c$ -axis orientation and the absence of in-plane epitaxial ordering. The SEM and FE-SEM images of Figure 3 allow us to conclude that the core/shell nanorods are densely packed, with a uniform morphology.

Significant insights into the core/shell nanorods structure were revealed using TEM and HR-TEM analyses, as discussed below. Regions of the samples containing hundreds of ZnO/ZnO core/shell nanorods were peeled off the Si(100) substrate using a surgical blade and mounted on the 300 mesh size TEM grid for analysis. Figure 4 shows TEM (Figure 4a) and HR-TEM (Figure 4b–d) images of the core/shell nanorods. The images in Figure 4a,b show that the nanorods have a core/shell structure with a crystalline (cr) core and an amorphous (am) shell. We now use the “cr-ZnO/am-ZnO core/shell” terminology to accurately refer to the established structure of the nanorods. Further detailed investigations were made at different locations of a specific core/shell nanorod, indicated by the circled regions marked “b”, “c”, and “d” in Figure 4a, corresponding to the images shown in Figure 4b–d. The inset of Figure 4b shows an HR-TEM image at the core/shell boundary region of the cr-ZnO/am-ZnO core/shell nanorods. These data confirm in greater detail the core/shell structure. An artificial line was drawn

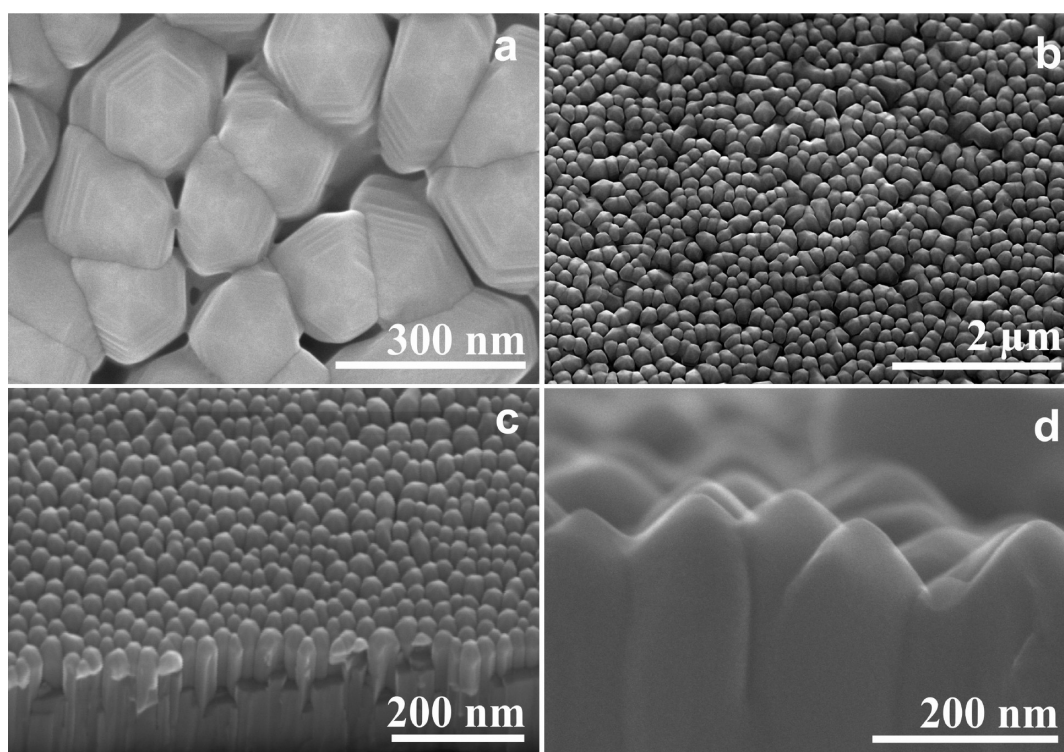


**Figure 3.** (a, b, d) Field emission SEM and (c) SEM images of ZnO/ZnO core/shell nanorods grown by PLD at (a) 0° tilt (plane view), (b) 20° tilt, (c) 30° tilt, and (d) 85° tilt angles.

as a guide to the eye in Figure 4b to show the crystalline core and amorphous shell regions. The cr-core/am-shell structure can be at least partially explained by the combination of several plausible factors such as the rate of material deposition prevailing in the PLD apparatus at the 800 °C substrate temperature, shadowing effects due to the compact nanorod distribution, and the final cooling rate. All of these factors may contribute to prevent the adatom diffusion necessary to find an equilibrium lattice site in the crystalline growth directions perpendicular to the *c*-axis. Additionally, we note that such cr-core/am-shell structures have also been produced serendipitously in previous works using different growth methods.<sup>17,19–21,24</sup>

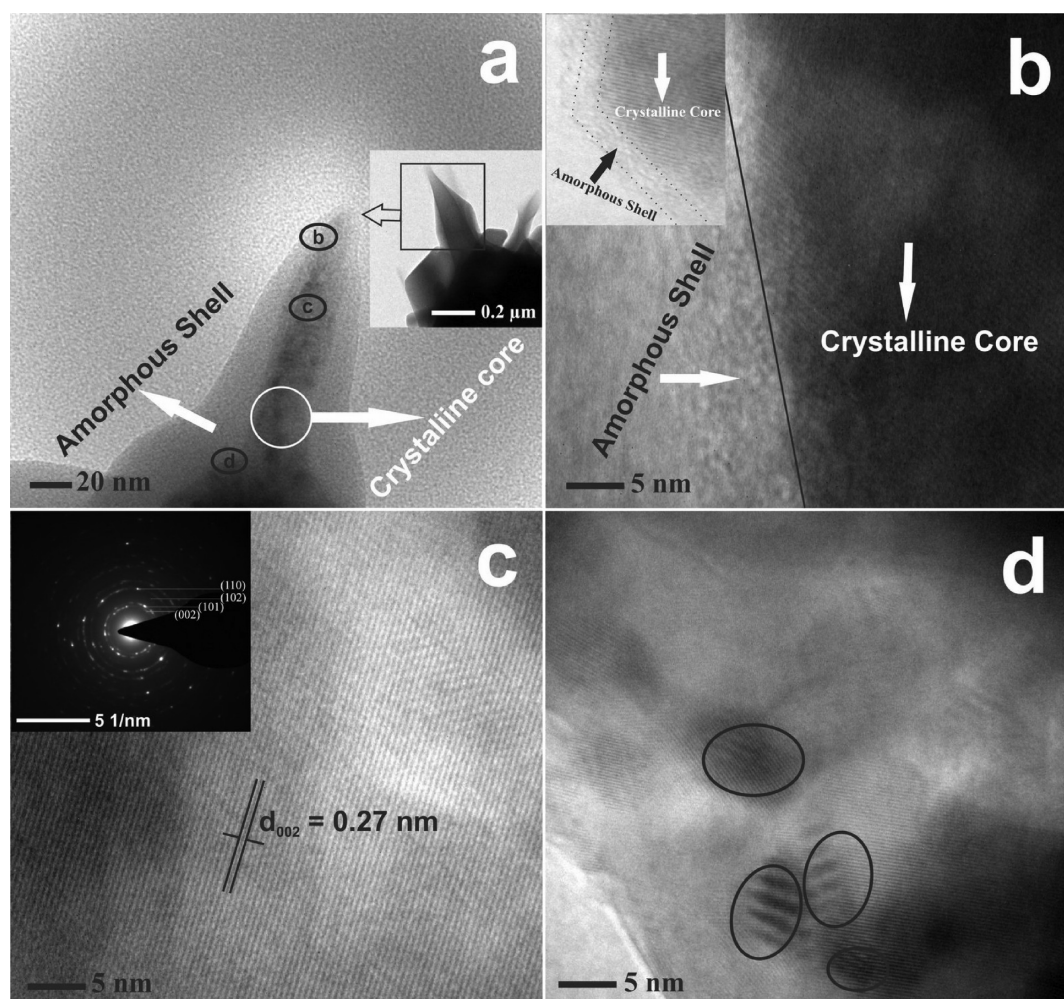
The HR-TEM image of the core part of the core/shell nanorods (indicated by the circled region c in Figure 4a) is represented in Figure 4c, and the observed lattice spacing from HR-TEM (0.27 nm) is in good agreement with that obtained from the XRD data above (0.26 nm). The selected area electron diffraction (SAED) pattern was collected using a 200 nm aperture and is shown in the inset of Figure 4c. The ring pattern in SAED indicates that the field of view contains polycrystalline material. The indexed (002), (101), (102), and (110) diffraction peaks belong to the pure ZnO phase and provide information complementary to the XRD pole figure data above. The HR-TEM data also allow us to identify specific regions at the interface between the crystalline core and amorphous shell, indicated by the circles (from the circled region d of Figure 4a) in Figure 4d which display clear evidence of Moiré fringes at the boundary. Li et al. identified no Moiré patterns in their HR-TEM data from PLD-grown ZnO/Er<sub>2</sub>O<sub>3</sub> core/shell nanorods, because their Er<sub>2</sub>O<sub>3</sub> shell region was polycrystalline.<sup>8</sup> Overall, the TEM and HR-TEM data clearly show that cr-ZnO/am-ZnO core/shell nanorods grown by PLD on Si(100) substrates have a core/shell structure (with a crystalline core and an amorphous shell) with Moiré fringes identified at the boundary region where structural

defects are expected, which may well be associated with the core/shell boundary interface region.

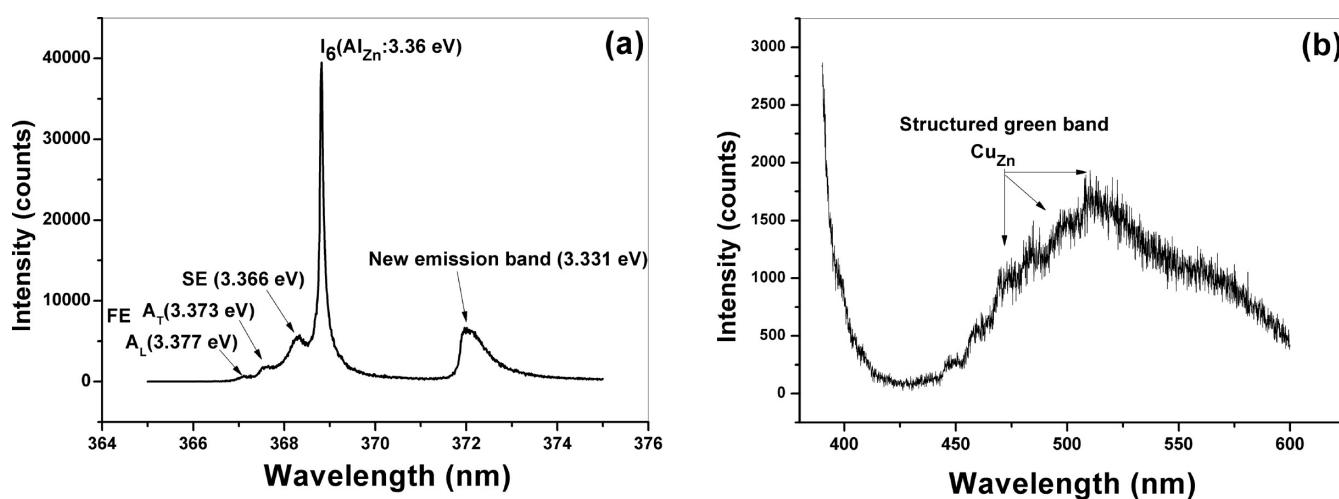
**3.3. Optical Properties.** Because of intrinsic and extrinsic defects/impurities, which lead to a range of donor/acceptor levels within the band gap, ZnO can emit light across the visible spectrum, as well as in the near-UV.<sup>38,39</sup> This is a key advantage for devices such as white light LEDs. However, the absence of stable and high hole mobility p-type material<sup>40</sup> remains the major obstacle for the development of large scale LEDs and laser diodes, and this, in turn, is due to the nature of the defect population in the material itself. In this regard, it remains of crucial importance to understand the defect population in this material, and a powerful tool for the study of such defects is their photoluminescence emission.

Figure 5 shows a typical low-temperature (13 K) PL spectrum of the cr-ZnO/am-ZnO core/shell nanorods produced in this work. Figure 5a reveals a strong I<sub>6</sub> line at 3.36 eV, which is generally attributed due to Al impurities, as well as a surface exciton (labeled SE) at 3.366 eV, and free exciton emission (labeled FE) at 3.377 eV (A<sub>L</sub>, longitudinal free exciton–polariton) and 3.373 eV (A<sub>T</sub>, transverse free exciton–polariton). Interestingly, an additional broad emission at 3.331 eV was also consistently observed in the low-temperature PL spectra of these samples. Defect-related emissions at 3.31, 3.3328, 3.3363, 3.333, and 3.3465 eV have been observed in various ZnO structures including bulk, single crystals, micro/nanocrystals, heterostructures, quantum dots, and one-dimensional structures (nanorods and nanowires), and also in p-type ZnO.<sup>41–46</sup> However, the present work identifies a new defect emission at 3.331 eV in these cr-ZnO/am-ZnO core/shell nanorods grown on ZnO buffer layers/Si(100) substrates by PLD. In a number of cases the emissions listed above have been associated with structural defects in ZnO crystals.<sup>41,42,44</sup> We note that, in previous articles, the emission lines observed at 3.3328 and 3.3363 eV in a ZnO





**Figure 4.** TEM, HR-TEM, and SAED images of cr-ZnO/am-ZnO core/shell nanorods grown by PLD. (a) TEM image of a core/shell nanorod. (b) Crystalline core and amorphous shell boundary region of a nanorod in the area indicated by circled b in (a). (c) HR-TEM image for the core part of a core/shell nanorod in the area indicated by circled c in (a). (d) Identified Moiré fringes in the area indicated by circled d in (a). The inset of (c) shows the SAED pattern of the area shown in (c).



**Figure 5.** Low temperature (13 K) PL spectra of cr-ZnO/am-ZnO core/shell nanorods: (a) near-band-edge region showing new emission band at 3.331 eV and (b) visible region showing structured green band emission.

single crystal are labeled as  $Y_0$  and  $Y_1$ , respectively.<sup>42</sup> Furthermore, the feature at 3.3328 eV ( $Y_0$ ) is also labeled in some publications as a DBX (donor bound exciton),<sup>47</sup> and as a

DD (deep donor bound exciton), emission.<sup>43,48</sup> The emission at 3.331 eV observed in this work is considerably broader (fwhm  $\sim$  1.75 meV) than the emissions observed in these other works

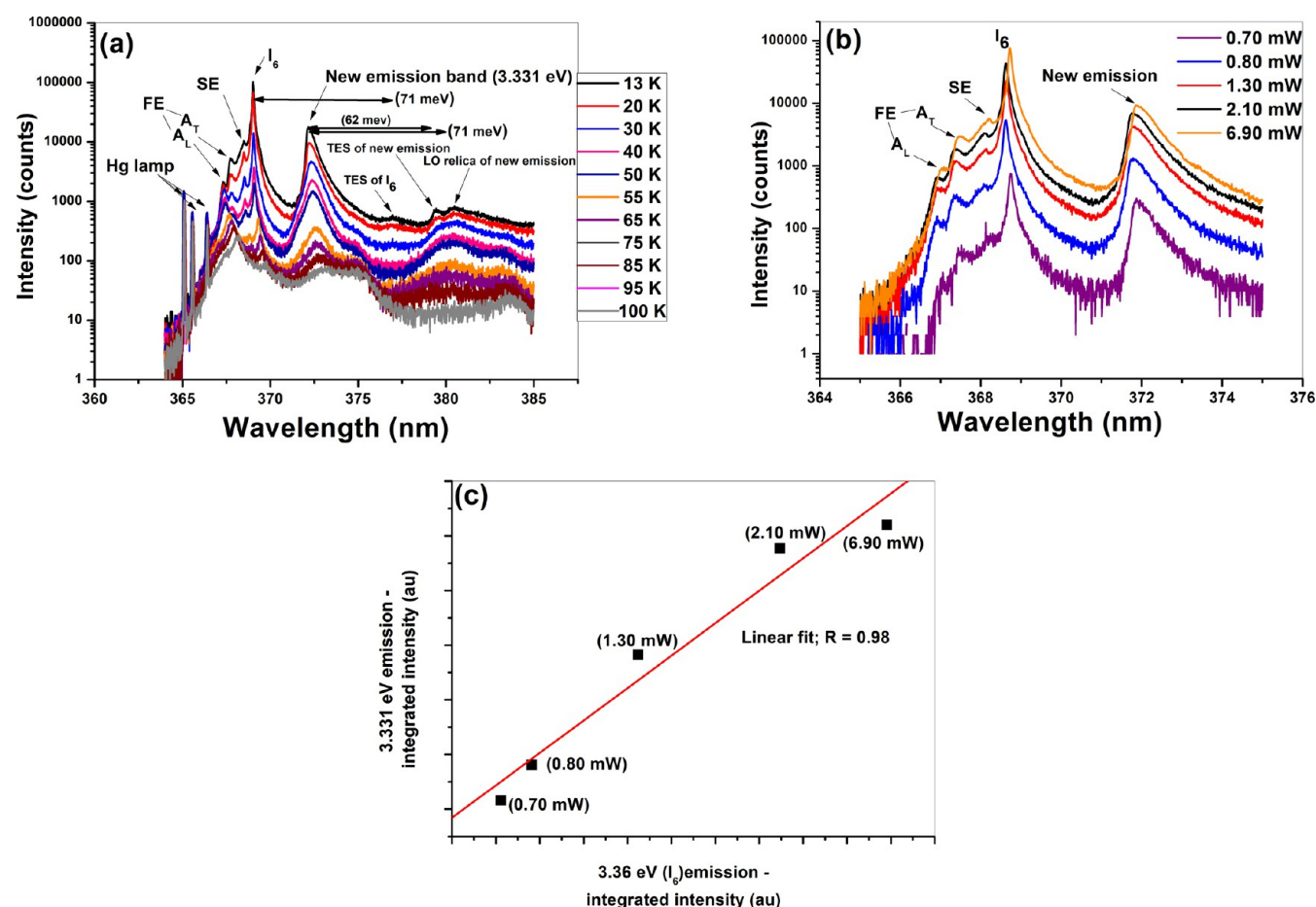


**Figure 6.** (a) Dependence of PL emission from cr-ZnO/am-ZnO core/shell nanorods on temperature. (b) Dependence of PL emission from cr-ZnO/am-ZnO core/shell nanorods on laser excitation power at constant temperature of 13 K. (c) Linear correlation between the integrated intensities of the  $I_6$  (3.36 eV) and 3.331 eV emission bands for the various laser powers used in this work.

(fwhm  $\sim 0.5$  and  $0.2$  meV),<sup>41,42</sup> as well as displaying a clearly asymmetric line shape. Deep level visible emission was also observed from the cr-ZnO/am-ZnO core/shell nanorods, as shown in Figure 5b, where the structured green band, due to Cu impurities, is clearly observed.<sup>49</sup>

The 3.331 eV emission was further investigated by varying the temperature and the laser excitation power. Figure 6a shows temperature dependent PL spectra from 13 to 100 K. We observed that as temperature increases the surface and shallow bound exciton emissions quench rapidly. It is clear that the initially strong  $I_6$  line reduces in intensity much faster compared to the 3.331 eV band. The 3.331 eV band can still be clearly seen at a temperature of 100 K, and this behavior implies involvement of deeply bound constituents, either an electron or a hole or both. Generally, two electron satellite (TES) and longitudinal optical (LO) replicas of the line are located in a region 30–70 meV from the parent emissions. However, since the 3.331 eV band still remains visible at a temperature (100 K) where the shallow bound exciton emission has been quenched, it is not due to a TES of the shallow bound exciton emission. We note that TES of the dominant  $I_6$  line and TES and an LO replica of the 3.331 eV emission are also observed in Figure 6a. These temperature dependent PL studies enable us to conclude that the 3.331 eV emission is stable up to 100 K and therefore it is neither a shallow bound exciton nor a TES or a phonon replica of a shallower bound exciton transition. It is therefore the zero phonon line associated with the recombination of deeply bound carriers at a defect in the material.

We have also varied the laser excitation power (using neutral density filters), at a fixed cryostat temperature of 13 K, as shown in Figure 6b. The 3.331 eV band remains visible and its shape is largely unchanged with varying power of the laser. Slight laser heating effects can just be distinguished at the highest laser power of 6.90 mW, where a small red shift in emission is seen across the entire near-band-edge region. It is however clearly observed in Figure 6c that the 3.331 eV band scales in a similar manner to the  $I_6$  shallow bound exciton emission with varying laser excitation power, even at the highest laser powers. This clearly demonstrates that the 3.331 eV emission is associated with a single electron–hole recombination, rather than a biexciton or other multielectron–hole pair crystal excitation, and the slight effects of laser heating at the highest laser power do not in any way affect this conclusion.

Based on the similarity in emission energy of the 3.331 eV band to that seen for other structural defect-related UV emissions,<sup>41,42,44</sup> and the simultaneous presence of structural defects at the boundary region of our core/shell nanorods, as revealed by HR-TEM data above (Figure 4d), we propose that the origin of the 3.331 eV band is electron–hole recombination at structural defects associated with the core/shell boundary interface region. This assignment is based on (i) the demonstrated presence of structural defects at the boundary region of the core/shell nanorods, as shown by HR-TEM, in samples which exhibit this 3.331 eV band emission; (ii) the deeper spectral position of the emission, similar to PL emissions

from other structural defects in ZnO, which is also consistent with the temperature stability of the emission; and (iii) the expected presence of structural defects with slightly different environments at the core/shell boundary region which explains the relatively large line width of the 3.331 eV emissions, since the slightly differing structural defect environments give rise to slight changes in emission energy from individual defects, and the ensemble effect yields the broader emission band observed in measurements.

#### 4. CONCLUSIONS

We have grown, for the first time, self-organized cr-ZnO/am-ZnO core/shell nanorods on Si(100) wafers by PLD, without using a metal catalyst seed and without the need for a separate growth stage for the shell region. This was achieved by using a specific sequence of heating and cooling phases pre- and postdeposition. The deposits were characterized using X-ray diffraction, electron microscopies, and photoluminescence. The characterization studies showed that the nanorods are highly textured with their *c*-axis oriented normal to, but without epitaxial in-plane ordering on, the substrate surface. The nanorods have conical terminations with rounded/blunt tips. They present a unique core/shell architecture with a crystalline core and an amorphous shell, while structural defects feature in the region of the core/shell boundary interface. The samples exhibit a previously unreported emission band at 3.331 eV in their low-temperature photoluminescence spectrum. This emission arises from a single electron–hole pair recombination involving deeply bound constituents likely associated with the structural defects at the core/shell boundary interface region.

The unique architecture and properties of the core/shell cr-ZnO/am-ZnO nanorods produced in this work should prove useful in applications where the functionality arises from the presence of an amorphous shell on a ZnO crystalline nanorod core. Examples of such applications would be in ZnO supercapacitor electrodes for energy storage, the passivation of ZnO photoanodes in dye-sensitized solar cells, or the control of the emission properties of ZnO nanolasers.

#### AUTHOR INFORMATION

##### Corresponding Author

\*E-mail: jean-paul.mosnier@dcu.ie. Tel: +353-17005303.

##### Author Contributions

The manuscript was written through contributions of all authors. All authors have given approval to the final version of the manuscript.

##### Notes

The authors declare no competing financial interest.

#### ACKNOWLEDGMENTS

S.I. acknowledges the award of a postgraduate studentship from INSPIRE (Integrated Nanoscience Platform for Ireland). This INSPIRE-funded work was conducted under the framework of the Irish Government's Programme for Research in Third Level Institutions Cycle 5, National Development Plan 2007–2013, with the assistance of the European Regional Development Fund. The authors also gratefully acknowledge Mr. Ciarán Gray and Dr. Joseph Cullen for their assistance with the low-temperature PL experiments, as well as Dr. Brendan Twamley for his help with the FE-SEM measurements.

#### ABBREVIATIONS

ZnO, zinc oxide; PLD, pulsed laser deposition; mT, millitorr; fwhm, full width at half-maximum; XRD, X-ray diffraction; PL, photoluminescence; FE-SEM, field emission scanning electron microscopy; TEM, transmission electron microscopy; HR-TEM, high resolution transmission electron microscopy; SAED, selected area electron diffraction; LED, light emitting diode; LO, longitudinal optical; TES, two electron satellite; DBX, donor bound exciton; DD, deep donor bound exciton

#### REFERENCES

- (1) Lee, C.; Chen, D. Large-scale synthesis of Ni-Ag core-shell nanoparticles with magnetic, optical and anti-oxidation properties. *Nanotechnology* **2006**, *17*, 3094–3099.
- (2) Zhu, Y. F.; Fan, A. H.; Shen, W. Z. A general chemical conversion route to synthesize various ZnO-based core/shell structures. *J. Phys. Chem. C* **2008**, *112*, 10402–10406.
- (3) Panda, S. K.; Dev, A.; Chaudhuri, S. Fabrication and luminescent properties of *c*-axis oriented ZnO-ZnS core-shell and ZnS nanorod arrays by sulfidation of aligned ZnO nanorod arrays. *J. Phys. Chem. C* **2007**, *111*, 5039–5043.
- (4) Gao, T.; Li, Q.; Wang, T. Sonochemical synthesis, optical properties, and electrical properties of core/shell-type ZnO nanorod/CdS nanoparticle composites. *Chem. Mater.* **2005**, *17*, 887–892.
- (5) Lin, Y.; Hung, Y.; Lin, H.; Tseng, Y.; Chen, Y.; Mou, C. Photonic crystals from monodisperse lanthanide-hydroxide-at-silica core/shell colloidal spheres. *Adv. Mater.* **2007**, *19*, 577–580.
- (6) Jang, J.; Nam, Y.; Yoon, H. Fabrication of polypyrrole-poly(*n*-vinylcarbazole) core-shell nanoparticles with excellent electrical and optical properties. *Adv. Mater.* **2005**, *17*, 1382–1386.
- (7) Caruso, F. Nanoengineering of particle surfaces. *Adv. Mater.* **2001**, *13*, 11–22.
- (8) Li, S. Z.; Gan, C. L.; Cai, H.; Yuan, C. L.; Guo, J.; Lee, P. S.; Ma, J. Enhanced photoluminescence of ZnO/Er<sub>2</sub>O<sub>3</sub> core-shell structure nanorods synthesized by pulsed laser deposition. *Appl. Phys. Lett.* **2007**, *90*, 263106.
- (9) Wang, Z. L. Novel nanostructures of ZnO for nanoscale photonics, optoelectronics, piezoelectricity, and sensing. *Appl. Phys. A: Mater. Sci. Process.* **2007**, *88*, 7–15.
- (10) Wang, Z.; Song, J. Piezoelectric nanogenerators based on zinc oxide nanowire arrays. *Science* **2006**, *312*, 242–246.
- (11) Liu, Y.; Zhong, M.; Shan, G.; Li, Y.; Huang, B.; Yang, G. Biocompatible ZnO/Au nanocomposites for ultrasensitive DNA detection using resonance Raman scattering. *J. Phys. Chem. B* **2008**, *112*, 6484–6489.
- (12) Si, S.; Li, C.; Wang, X.; Peng, Q.; Li, Y. Fe<sub>2</sub>O<sub>3</sub>/ZnO core-shell nanorods for gas sensors. *Sens. Actuators, B* **2006**, *119*, 52–56.
- (13) Huang, B.; Lin, J. Core-shell structure of zinc oxide/indium oxide nanorod based hydrogen sensors. *Sens. Actuators, B* **2012**, *174*, 389–393.
- (14) Schrier, J.; Demchenko, D. O.; Wang, L. Optical properties of ZnO/ZnS and ZnO/ZnTe heterostructures for photovoltaic applications. *Nano Lett.* **2007**, *7*, 2377–2382.
- (15) Greene, L. E.; Law, M.; Yuhas, B. D.; Yang, P. ZnO-TiO<sub>2</sub> core-shell nanorod/P3HT solar cells. *J. Phys. Chem. C* **2007**, *111*, 18451–18456.
- (16) Kanmani, S. S.; Ramachandran, K. Synthesis and characterization of TiO<sub>2</sub>/ZnO core/shell nanomaterials for solar cell applications. *Renewable Energy* **2012**, *43*, 149–156.
- (17) Wang, M.; Huang, C.; Cao, Y.; Yu, Q.; Guo, W.; Huang, Q.; Liu, Y.; Huang, Z.; Huang, J.; Wang, H.; et al. The effects of shell characteristics on the current-voltage behaviors of dye-sensitized solar cells based on ZnO/TiO<sub>2</sub> core/shell arrays. *Appl. Phys. Lett.* **2009**, *94*, 263506.
- (18) Li, G.; Wang, Z.; Zheng, F.; Ou, Y.; Tong, Y. ZnO@MoO<sub>3</sub> core/shell nanocables: Facile electrochemical synthesis and enhanced supercapacitor performances. *J. Mater. Chem.* **2011**, *21*, 4217–4221.



- (19) Yang, P.; Xiao, X.; Li, Y.; Ding, Y.; Qiang, P.; Tan, X.; Mai, W.; Lin, Z.; Wu, W.; Li, T.; et al. Hydrogenated ZnO core-shell nanocables for flexible supercapacitors and self-powered systems. *ACS Nano* **2013**, *7*, 2617–2626.
- (20) Xia, X.; Tu, J.; Zhang, Y.; Wang, X.; Gu, C.; Zhao, X.; Fan, H. J. High-quality metal oxide core/shell nanowire arrays on conductive substrates for electrochemical energy storage. *ACS Nano* **2012**, *6*, 5531–5538.
- (21) Wang, Z.; Guo, R.; Li, G.; Ding, L.; Ou, Y.; Tong, Y. Controllable synthesis of ZnO-based core/shell nanorods and core/shell nanotubes. *RSC Adv.* **2011**, *1*, 48–51.
- (22) Trejo, M.; Santiago, P.; Sobral, H.; Rendon, L.; Pal, U. Synthesis and growth mechanism of one-dimensional Zn/ZnO core-shell nanostructures in low-temperature hydrothermal process. *Cryst. Growth Des.* **2009**, *9*, 3024–3030.
- (23) Zeng, H.; Cai, W.; Cao, B.; Hu, J.; Li, Y.; Liu, P. Surface optical phonon Raman scattering in Zn/ZnO core-shell structured nanoparticles. *Appl. Phys. Lett.* **2006**, *88*, 181905.
- (24) Zhou, H.; Alves, H.; Hofmann, D.; Kriegseis, W.; Meyer, B.; Kaczmarczyk, G.; Hoffmann, A. Behind the weak excitonic emission of ZnO quantum dots: ZnO/Zn(OH)<sub>2</sub> core-shell structure. *Appl. Phys. Lett.* **2002**, *80*, 210–212.
- (25) Kaydashev, V. E.; Kaidashev, E. M.; Peres, M.; Monteiro, T.; Correia, M. R.; Sobolev, N. A.; Alves, L. C.; Franco, N.; Alves, E. Structural and optical properties of Zn<sub>0.9</sub>Mn<sub>0.1</sub>O/ZnO core-shell nanowires designed by pulsed laser deposition. *J. Appl. Phys.* **2009**, *106*, 093501.
- (26) Mosnier, J. P.; O'Haire, R. J.; McGlynn, E.; Henry, M. O.; McDonnell, S. J.; Boyle, M. A.; McGuigan, K. G. ZnO films grown by pulsed-laser deposition on soda lime glass substrates for the ultraviolet inactivation of *Staphylococcus epidermidis* biofilms. *Sci. Technol. Adv. Mater.* **2009**, *10*, 045003.
- (27) Klingshirn, C. F.; Meyer, B. K.; Waag, A.; Hoffmann, A.; Geurts, J. In *Zinc Oxide—From Fundamental Properties Towards Novel Applications*; Hull, R., Jagadish, C., Osgood, R. M., Parisi, J., Wang, Z., Warlimount, H., Eds.; Springer: Berlin, 2010; Vol. 120, Chapter 3, pp 66–67.
- (28) Tien, L. C.; Pearton, S. J.; Norton, D. P.; Ren, F. Synthesis and microstructure of vertically aligned ZnO nanowires grown by high-pressure-assisted pulsed-laser deposition. *J. Mater. Sci.* **2008**, *43*, 6925–6932.
- (29) Willander, M.; Nur, O.; Zhao, Q. X.; Yang, L. L.; Lorenz, M.; Cao, B. Q.; Perez, J. Z.; Czekalla, C.; Zimmermann, G.; Grundmann, M.; et al. Zinc oxide nanorod based photonic devices: recent progress in growth, light emitting diodes and lasers. *Nanotechnology* **2009**, *20*, 332001.
- (30) In *Pulsed Laser Deposition of Thin Films: Applications-Led Growth of Functional Materials*; Eason, R., Ed.; Wiley: Hoboken, NJ, 2007; Chapter 8, pp 177–180, and Chapter 12, pp 268–282.
- (31) Kumar, R. T. R.; McGlynn, E.; McLoughlin, C.; Chakrabarti, S.; Smith, R. C.; Carey, J. D.; Mosnier, J. P.; Henry, M. O. Control of ZnO nanorod array density by Zn supersaturation variation and effects on field emission. *Nanotechnology* **2007**, *18*, 215704.
- (32) McCarthy, E.; Kumar, R. T. R.; Doggett, B.; Chakrabarti, S.; O'Haire, R. J.; Newcomb, S. B.; Mosnier, J. P.; Henry, M. O.; McGlynn, E. Effects of the crystallite mosaic spread on integrated peak intensities in 2 theta-omega measurements of highly crystallographically textured ZnO thin films. *J. Phys. D: Appl. Phys.* **2011**, *44*, 375401.
- (33) Wan, W.; Zhu, L.; Hu, L.; Chen, G.; Mi, W.; Ye, Z. Investigation of morphology evolution of Cu-ZnO nanorod arrays and enhancement of ferromagnetism by codoping with N. *Phys. Lett. A* **2014**, *378*, 2763–2767.
- (34) Mote, V. D.; Purushotham, Y.; Dole, B. N. Williamson-Hall analysis in estimation of lattice strain in nanometer-sized ZnO particles. *J. Theor. Appl. Phys.* **2012**, *6*, 1–8.
- (35) Jie, J.; Wang, G.; Chen, Y.; Han, X.; Wang, Q.; Xu, B.; Hou, J. Synthesis and optical properties of well-aligned ZnO nanorod array on an undoped ZnO film. *Appl. Phys. Lett.* **2005**, *86*, 031909.
- (36) Teki, R.; Parker, T. C.; Li, H.; Koratkar, N.; Lu, T.; Lee, S. Low temperature synthesis of single crystalline ZnO nanorods by oblique angle deposition. *Thin Solid Films* **2008**, *516*, 4993–4996.
- (37) Morkoç, H.; Özgür, Ü. In *Zinc Oxide—Fundamentals, Materials and Device Technology*; Wiley-VCH: Weinheim, Germany, 2009; Chapters 1 and 2.
- (38) Djurisić, A.; Leung, Y.; Tam, K.; Ding, L.; Ge, W.; Chen, H.; Gwo, S. Green, yellow, and orange defect emission from ZnO nanostructures: Influence of excitation wavelength. *Appl. Phys. Lett.* **2006**, *88*, 103107.
- (39) Liu, W.; Gu, S.; Ye, J.; Zhu, S.; Liu, S.; Zhou, X.; Zhang, R.; Shi, Y.; Zheng, Y.; Hang, Y.; et al. Blue-yellow ZnO homostructural light-emitting diode realized by metalorganic chemical vapor deposition technique. *Appl. Phys. Lett.* **2006**, *88*, 092101.
- (40) Look, D. C.; Claflin, B.; Alivov, Y.; Park, S. The future of ZnO light emitters. *Phys. Status Solidi A* **2004**, *201*, 2203–2212.
- (41) Schirra, M.; Schneider, R.; Reiser, A.; Prinz, G. M.; Feneberg, M.; Biskupek, J.; Kaiser, U.; Krill, C. E.; Thonke, K.; Sauer, R. Stacking fault related 3.31-eV luminescence at 130-meV acceptors in zinc oxide. *Phys. Rev. B* **2008**, *77*, 125215.
- (42) Wagner, M. R.; Callsen, G.; Reparaz, J. S.; Schulze, J.-H.; Kirste, R.; Cobet, M.; Ostapenko, I. A.; Rodt, S.; Nenstiel, C.; Kaiser, M.; et al. Bound excitons in ZnO: Structural defect complexes versus shallow impurity centers. *Phys. Rev. B* **2011**, *84*, 035313.
- (43) Johnston, K.; Henry, M.; McCabe, D.; McGlynn, E.; Dietrich, M.; Alves, E.; Xia, M. Identification of donor-related impurities in ZnO using photoluminescence and radiotracer techniques. *Phys. Rev. B* **2006**, *73*, 165212.
- (44) Alves, H.; Pfisterer, D.; Zeuner, A.; Riemann, T.; Christen, J.; Hofmann, D.; Meyer, B. Optical investigations on excitons bound to impurities and dislocations in ZnO. *Opt. Mater.* **2003**, *23*, 33–37.
- (45) Reynolds, J. G.; Reynolds, C. L., Jr.; Mohanta, A.; Muth, J. F.; Rowe, J. E.; Everitt, H. O.; Aspnes, D. E. Shallow acceptor complexes in p-type ZnO. *Appl. Phys. Lett.* **2013**, *102*, 152114.
- (46) Lange, M.; Zippel, J.; Benndorf, G.; Czekalla, C.; Hochmuth, H.; Lorenz, M.; Grundmann, M. Temperature dependence of localization effects of excitons in ZnO/Cd<sub>x</sub>Zn<sub>1-x</sub>O/ZnO double heterostructures. *J. Vac. Sci. Technol., B* **2009**, *27*, 1741–1745.
- (47) Meyer, B.; Alves, H.; Hofmann, D.; Kriegseis, W.; Forster, D.; Bertram, F.; Christen, J.; Hoffmann, A.; Strassburg, M.; Dworzak, M.; et al. Bound exciton and donor-acceptor pair recombinations in ZnO. *Phys. Status Solidi B* **2004**, *241*, 231–260.
- (48) Schildknecht, A.; Sauer, R.; Thonke, K. Donor-related defect states in ZnO substrate material. *Physica B: Condens. Matter* **2003**, *340*, 205–209.
- (49) Byrne, D.; Herklotz, F.; Henry, M. O.; McGlynn, E. Unambiguous identification of the role of a single Cu atom in the ZnO structured green band. *J. Phys.: Condens. Matter* **2012**, *24*, 215802.